JSS Focus Issue on Gallium Oxide Based Materials and Devices

Electronic Structure of Tungsten-Doped β-Ga_2O_3 Compounds

Vishal Zade,[1] B. Mallesham,[1] Swadipta Roy,[1,2] V. Shutthanandan,[2] and C. V. Ramana [1,z]

[1] *Center for Advanced Materials Research (CMR), University of Texas at El Paso, El Paso, Texas 79968, USA*
[2] *Environmental Molecular Sciences Laboratory (EMSL), Pacific Northwest National Laboratory (PNNL), Richland, Washington 99352, USA*

Tungsten (W) doped gallium oxide (Ga_2O_3) ($Ga_{2-2x}W_xO_3$, $0.00 \leq x \leq 0.30$, GWO) polycrystalline ceramic compounds were synthesized via conventional, high-temperature solid-state reaction method. The effect of W-doping on the crystal structure and electronic structure of the resulting GWO materials is studied in detail. The GWO compounds were single-phase, crystallized in β-Ga_2O_3 for $x \leq 0.15$, at which point the Ga_2O_3-WO_3 composite formation occurs. The average crystallite size increases with increasing W-content; however, the effect is predominant only in the single phase GWO compounds. Corroborating with structural analyses, the X-ray photoelectron spectroscopy (XPS) measurements reveal the chemical state of W ions vary in GWO compounds as a function of W concentration. The mixed chemical valence states of W (W^{4+} and W^{6+}) were evident in single-phase GWO compounds where the W-concentration is lower. However, W ions exhibit the highest chemical valence state (W^{6+}) for higher x values, which resulted in the Ga_2O_3-WO_3 composite formation. The Ga ions exists in their highest chemical valence state (Ga^{3+}) in all of the GWO compounds. The scientific understanding of the electronic structure of the GWO materials derived as function of W concentration could be useful while considering the W-doped Ga_2O_3 materials and/or W-Ga_2O_3 contacts for electronic and optoelectronic device applications.
 [DOI: 10.1149/2.0121907jss]

Manuscript received February 5, 2019. Published March 8, 2019. *This paper is part of the JSS Focus Issue on Gallium Oxide Based Materials and Devices.*

Gallium oxide (Ga_2O_3), which is currently the most popular among wide bandgap transparent oxides, is potentially applicable in a broad range of optical, electronic, optoelectronic applications.[1–5] The unique properties coupled with chemical and thermal stability makes β-Ga_2O_3 and related materials fascinating to work with a range of technological applications, which expand to high power electronic devices,[5,6] solar blind UV-photodetectors,[7,8] light emitting diodes,[2,9,10] photocatalysts,[11] transparent conducting oxides (TCOs),[12–14] and chemical sensors.[15–17] β-Ga_2O_3 is the second largest wide bandgap material with a bandgap of ~4.9 eV.[18] The predicted breakdown strength is rather high (8 MV/cm) in β-Ga_2O_3.[19,20] Thus, due to its large bandgap and high breakdown strength, β-Ga_2O_3 has the potential to out preform Si, GaN and SiC in power electronics.

Recently, doping of β-Ga_2O_3 with rare-earth (RE) or transition metal (TM) ions has been considered widely in the literature. The attention directed toward using RE-ions was primarily toward improving the luminescence and electroluminescence properties while TM-ion doping was particularly to engineer the optical or electrical or optoelectronic properties. The crystal symmetry of β-Ga_2O_3 is monoclinic (space group: C2/m) with cell parameters, $a = 12.214$, $b = 3.0371$, $c = 5.7981$ Å and $\beta = 103.83°$.[21] In monoclinic unit cell, Ga occupies either with the tetrahedrally coordinated oxygens and or with the octahedrally coordinated oxygens.[21,22] On the other hand, oxygen assumes three different lattice sites in distorted cubic close packed arrangement around Ga sites.[21] Thus, manipulation of structure and/or defects by suitable dopants into β-Ga_2O_3 provides ability to engineer properties with application. For instance, Si doping into β-Ga_2O_3 enables to control the overall electrical conductivity.[23] Substituting Si^{4+} at Ga site works effectively as an electron donor resulting in an increased *n*-type conductivity in contrast to undoped Ga_2O_3. The tunable electrical characteristics, namely the carrier density and electrical resistivity, were demonstrated in Sn doped Ga_2O_3 single crystals.[8] Studies made using Density Functional Theory calculations on the effect of transition metal ions into β-Ga_2O_3 reports that W, Mo and Re act as deep donors, whereas Nb, with its lower formation energy acts as a shallow donor.[24] W and Ti doped β-Ga_2O_3 polycrystalline thin films exhibited a red-shift in optical bandgap.[7,25–27] The present work was directed toward the fundamental, scientific understanding of the electronic structure of W-doped Ga_2O_3 (GWO) bulk ceramics. The obvious relevance and consideration of the GWO system in this work is due to the following reasons. Shannon ionic radii of W^{6+} (tetrahedral – 0.040 nm and octahedral - 0.060 nm) and Ga^{3+} (tetrahedral – 0.047 nm and octahedral - 0.062 nm)[28] both in tetrahedral and octahedral coordination provide comparable proximity coupled with resemblance in electronegativity (Ga-1.82,[29] W-2.36[30]) values. All these factors strongly indicate that the parent crystal structure can be preserved while tuning the electronic properties. Furthermore, W metal contacts have been proposed for Ga_2O_3 based power electronic devices.[31,32] Understanding of the W-doped Ga_2O_3 could be useful to predict the surface/interface diffusion and reaction compounds (if any) in such device applications involving W-Ga_2O_3 contacts. Also, the GWO bulk ceramic materials with controlled structure and properties may be useful to employ them as target materials for high-quality thin film deposition using physical vapor deposition. Therefore, GWO bulk ceramics were produced using the simple, versatile high-temperature solid state chemical reaction method. The crystal structure and electronic properties of the resulting materials were studied as a function of W concentration and the results are reported in this paper.

Experimental

Conventional solid-state reaction method was employed to synthesize $Ga_{2-2x}W_xO_3$ (GWO) bulk ceramics varying composition in the range $0 \leq x \leq 0.30$. High pure metal oxide powder precursors Ga_2O_3 (99.99%) and WO_3 (99.9% purity) were procured from Sigma Aldrich. Each compound was synthesized form the powder precursors in stoichiometric proportions. The powders in stochiometric proportions were pulverized in an agate mortar with the help of acetone as a wetting media. Once homogeneity is attained, the thoroughly missed powders were calcined at 1050°C for 12 hours and then at 1150°C for another 12 hours) in a muffle furnace. Each step was followed by intermediate grinding to assist a complete solid-state reaction. It also assists in reducing the particle size and gives an enhanced siterability. Post calcination, binder (Poly vinyl alcohol (PVA)) was added to the pulverized powders and circular pellets were made (8 mm diameter; 1 mm thickness) using a uniaxial hydraulic press by applying load of

[z] E-mail: rvchintalapalle@utep.edu

1.5 ton. These green pellets were sintered at 1250°C for 6 h with a ramp rate of 5°C and binder burnout of pellets was carried out at a holding temperature of 500°C for 30 min.

The GWO bulk ceramics were analyzed with X-ray diffraction (XRD) to better understand the crystal structure of the system. The XRD patterns were collected using Rigaku Benchtop powder X-ray diffractometer (Mini Flex II). Scanning parameters were: 10° – 80°(2θ range), step size – 0.02° and Scan rate – 0.6°/min. X-ray photoelectron spectroscopic (XPS) scan of the GWO ceramics were obtained employing Kratos Axis Ultra DLD spectrometer using Al Kα monochromatic X-ray source (1486.6 eV) and a high-resolution hemispherical analyzer. The X-ray source power was set at 105 W. Emitted photoelectrons were collected by the detector aligned normally to the sample surface. XPS data were obtained from an area of 700 × 300 μm.[2] The survey and high-resolution scans were carried out at a pass energy of 160 and 20 eV respectively. The step size used for the survey scan was 0.5 eV while for the high-resolution scans step size of 0.1 eV was considered for obtaining the data. The high-resolution scan at 20 eV pass energy was calibrated employing a standard Ag sample which produced a full width half-maxima (FWHM) of 0.59 eV for the Ag $3d_{5/2}$ core level. Samples were mounted on the XPS stub using double sided Cu tape. Charge neutralizer was set at a value of 4.2 eV as these are insulating ceramic oxide samples. Data were analyzed with the help of CasaXPS software employing Gaussian/Lorentzian (GL(30)) line shape, line asymmetry and Shirley background correction. Survey scans were collected over the binding energy (B.E.) range of 1400-(-) 5 eV. High resolution spectra of Ga 2p, O 1s, C 1s, W 4f and Ga 3d peak regions were obtained with at least 16 number of sweeps for each of them depending on the clarity of the peaks. Though both the Ga peaks (i.e. Ga 2p and 3d) were collected for confirmation, but only Ga 2p spectra is depicted in order to avoid the clumsiness coming from the interference of Ga 3d peak with O 2s peak as both the peaks are very closely spaced. Before the collection of respective XPS spectra, sample surfaces were thoroughly cleaned using ultraviolet ozone cleaner for a duration of 5 min to remove any type of contamination, especially from hydro-carbons and then the samples were loaded into the XPS chamber for analysis. The binding energy of carbon (C 1s) peak at 284.8 eV was used as the charge reference for all the high-resolution spectra. For each sample at least three positions were scanned for both survey and high-resolution spectra to check the uniformity of the compounds and for maintaining the statistical index.

Results and Discussion

The XRD pattern of GWO ceramic compounds are shown in Fig. 1. The peaks were indexed to β-Ga_2O_3.[21] It is evident from the XRD patterns that the W-doped Ga-oxide samples also crystallize in single-phase β-Ga_2O_3 for a W concentration of $x = 0.15$. However, at $x>0.15$, WO_3 secondary phase formation occurs resulting in a Ga_2O_3-WO_3 composite. Asterisks in Fig. 1 indicate the diffraction peaks due to WO_3. It is important to recognize that, based on the XRD patterns, the β-Ga_2O_3 is dominant phase in the Ga_2O_3-WO_3 composite. The amount of secondary phase of WO_3 is limited to 2–9%, the highest (9%) is noted only in the samples for $x = 0.30$. However, this result is due to the final sintering in the two-step calcination process, which indicate that the secondary phase formation is quite high in the first step of calcination, adopted as reported and discussed elsewhere.[33] Furthermore, detailed assessment and analyses of (400), (110) and (111) peaks indicate a minor but positive shift with increasing W concentration to $x = 0.15$. This is, perhaps, due to smaller ionic radius of W^{6+}, as compared to Ga^{3+}, leading to the unit cell volume reduction upon W ion incorporation in β-Ga_2O_3. It may be noted that the magnitude of peak shift is non-uniform for different Bragg Planes. Thus, the XRD peaks and characteristic peak shift indicate the formation of GWO solid solution for $x \leq 0.10$. We believe that the stark difference in the formation enthalpies[33] of WO_3[24] and Ga_2O_3[24] must be a factor which limits the W-solubility at Ga site to less than 10 at%. Note that W melts at 3422°C while WO_3 melts correspondingly at 1473°C.[33,34] Reports have assessed the incongruent nature of

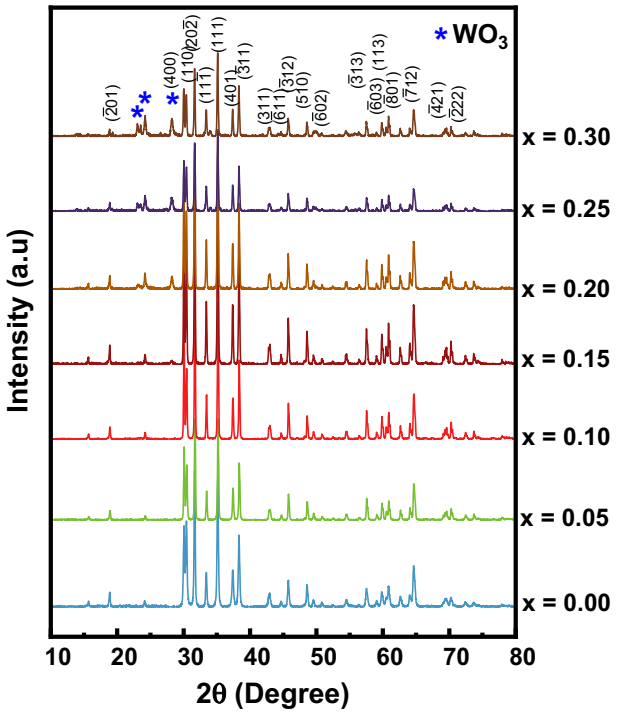

Figure 1. XRD patterns of GWO compounds. Evident from the XRD patterns, the W-doped Ga-oxide samples crystallize in single-phase β-Ga_2O_3 for a W concentration of $x = 0.15$. At $x>0.15$, WO_3 secondary phase formation occurs resulting in Ga_2O_3-WO_3 composite as indicated by the presence of the addition peaks.

WO_2 melting at 1530°C to a two-phase field of W-$W_{18}O_{49}$.[35] A number of W oxides can be observed for WO_2 and WO_3 (e.g., $W_{18}O_{49}$ and W_nO_{3n-2}) with corresponding liquidus and eutectic temperatures in the range of 1430°C and 1600°C However, for our case, the series of W_nO_{3n-2} phases can be avoided so as to simply focus on the effect of WO_3. In a Ga-W-O ternary system, liquid Ga will be confined in a three-phase field of Ga_2O_3-W-liquid. In a Ga-W-O ternary system and phase equilibria, liquid Ga occurs in a small region on the lower right side of the Ga-W-O system and bounded by a three-phase field of Ga_2O_3-W-liquid. The two-phase field of Ga_2O_3-WO_3 on the calculated ternary phase diagram does not show a liquid region. Therefore, under the GWO ceramic processing temperature of 1250°C, which is well below or far from these melting temperatures of various components discussed, we believe that the W incorporation into β-Ga_2O_3 is facilitated by the substitution of W-ions at the Ga-ions while the formation of vacancies may be the driving factor for the mass transport. Under such circumstances, the β-Ga_2O_3 can adopt only certain amount of dopant concentration while the dopant oxide phase evolves as a secondary phase leading to the composite or mixed oxide formation at higher concentrations. These thermodynamic considerations can, therefore, account for the observed single-phase β-Ga_2O_3 with W solubility as well as mixed oxide of Ga_2O_3-WO_3 composite as a function of variable W concentration.

In order to understand the effect of W-content on the crystal growth, the average crystallite size of the GWO compounds is determined using Debye Scherrer relation:

$$D = \frac{0.9\lambda}{\beta \cos\theta} \quad [1]$$

where, D – Crystallite size, λ ($Cu_{K\alpha}$) - 1.5406 Å, β - Full width at half maximum, θ – diffraction angle. The variation of the average crystallite size with W-concentration in GWO compounds is presented in Fig. 2. It is evident that the crystallite size increases with W incorporation. However, the size increase is considerably higher in the samples that corresponds to single phase GWO compounds i.e., with complete

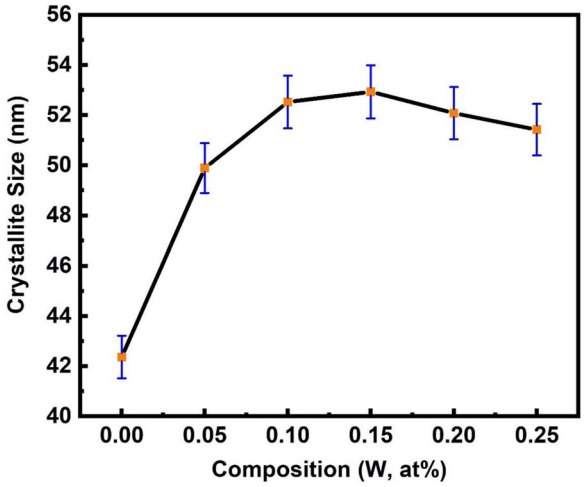

Figure 2. Variation of the average crystallite size with W-concentration in GWO compounds.

solubility of W ions. For intrinsic Ga_2O_3, the crystallite size estimated is ~40 nm, which increases to ~50 nm for W-doped Ga_2O_3 samples with $x = 0.05$. Further increase in W concentration up to $x = 0.15$ resulted in a slight increase in the crystallite size. However, further increase in W-concentration beyond $x = 0.15$ didn't induce appreciable change; in fact, the GWO samples with higher W-content reveal an average crystallite size of ~50 nm within the experimental error.

Being a surface sensitive characterization technique X-ray photoelectron spectroscopy (XPS) is employed to understand the surface chemistry of the as prepared GWO sintered compounds and the chemical valence state(s) of the constituent elements. The XPS survey spectra of GWO ceramics are presented in Fig. 3. It is evident from the spectra that Ga, W and O are the constituent elements. The presence of C *1s* peak in the spectra is due to fortuitous carbon which occurs due to exposure air after synthesis and just before the samples are places in the XPS system. Therefore, the spectra were calibrated to the C *1s* peak at a binding energy (BE) of 284.8 eV.

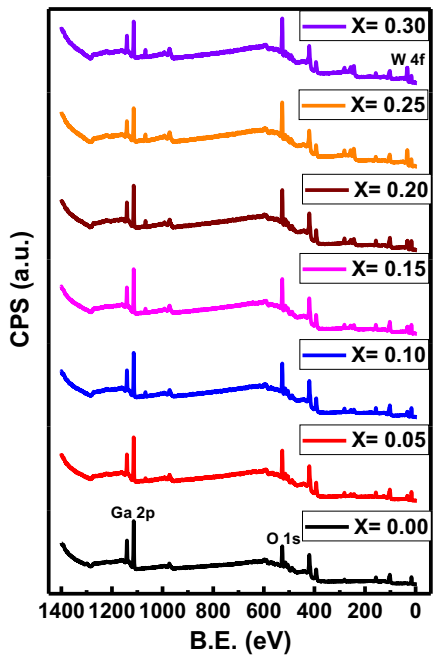

Figure 3. XPS survey spectra of GWO compounds.

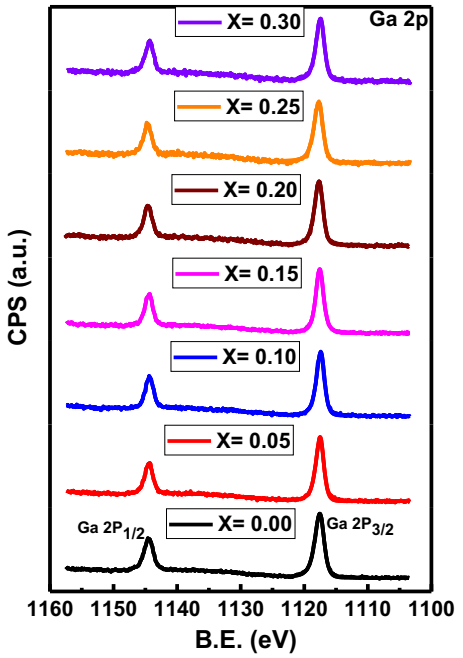

Figure 4. Ga 2p core level XPS spectra of GWO compounds.

The XPS core level spectra of Ga 2*p* region are presented in Fig. 4. It is evident that the Ga 2*p* region (Fig. 4) comprises of Ga 2p doublet i.e., the Ga $2p_{3/2}$ and Ga $2p_{1/2}$ peaks, which are located about at BEs of 1117.5 and 1144.2 eV, respectively. The Ga $2p_{3/2}$ component is located at a BE of 1116.7 eV for Ga metal.[36] Thus, compared to the Ga metallic state, the observed Ga $2p_{3/2}$ peak shows a positive BE shift indicating that the Ga ions exist in their higher valence state. The BE positive shift in the BE of Ga $2p_{3/2}$ peak is due to the redistribution of the electronic charge, because Ga chemical state is stabilized as Ga_2O_3 in the GWO compounds. No changes in BE location and/or peak shape were observed for the Ga 2*p* region as a function of variable W-concentration in the GWO compounds. Thus, the observed more or less same BE and peak shape without any appreciable change in the Ga 2*p* core-level XPS data, which are consistent with the reported values in the literature for Ga_2O_3, validates the claim that Ga ions exist in the highest valence states (i.e., Ga^{3+}) in all the GWO compounds.

A detailed core-level spectra of W *4f* for GWO sintered compounds are shown in Fig. 5. A well-resolved doublet corresponding to W $4f_{5/2}$ at BE ~ 37.5 eV and W $4f_{7/2}$ at BE ~ 35.4 eV can be observed in Fig. 5. The W $4f_{7/2}$ peak at 35.4 eV corroborates with the literature (35.4 eV) and also characterizes the W^{6+} state in WO_3. However, it is noted that W *4f* doublet exhibits slight peak broadening for GWO samples with lower W concertation. This observation indicates that a few W ions exhibit lower valence state. The deconvoluted W 4*f* core-level XPS spectra and peak fitting indicate a mixture of W^{4+} and W^{6+} valence states for lower W-concentration. However, this is predominant only in GWO samples with $x = 0.05$ although the presence of these components exists up to $x = 0.15$. With further increase in x values, the core-level W *4f* spectra indicate that the component corresponding to lower valence state of W ions disappears fully. However, the $x = 0.30$ GWO compound shows a shift of 0.30 eV for the W 4f peak which can be due to the multiple intermediate steps involved in the sample fabrication method such as palletization, proper control of the furnace atmosphere and maintaining stoichiometry etc. The XPS data of W fully corroborates with the observations made from XRD. The W incorporation into β-Ga_2O_3 is facilitated by the substitution of W-ions at the Ga-ions. However, due to charge imbalance, some of the W-ions may exists at lower valence state although such lower valence state of W is not reflected in XRD due to the fact that it is minor. In fact, formation of W ions with different chemical valence

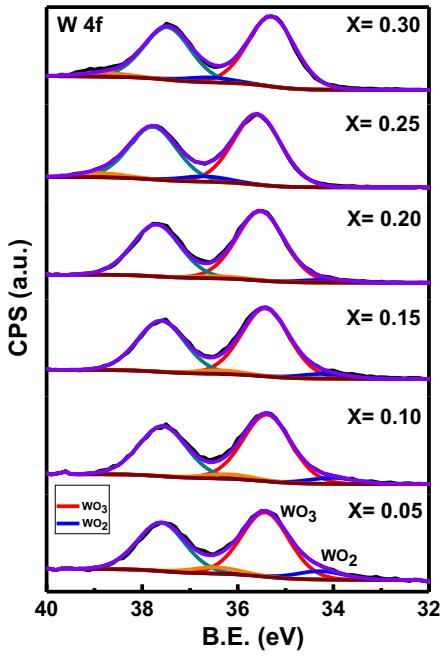

Figure 5. W 4f core level XPS spectra of GWO compounds.

may assist the mass transportation and sintering of the GWO ceramics. Therefore, as observed in XRD, the β-Ga_2O_3 can adopt only certain amount of W-concentration while the fully stabilized W-oxide phase evolves as a secondary phase leading to the composite or mixed oxide formation at higher concentrations. This is evident in the XPS data, where the lower valence state disappears when Ga_2O_3-WO_3 composite formation occurs at higher W concentration.

The O 1*s* peak (Fig. 6) at BE of 530.5 eV, is the characteristic feature of Ga-O bonds in Ga_2O_3.[37–39] It must be noted that the O 1*s* peak is asymmetrical for the GWO compounds. Three components representing different chemical states are evident from the O 1*s* peak fitting. The most intense peak, centered at B.E. of 530.5 eV is the characteristic peak of oxygen bonded to either Ga or W within the GWO compound. The higher BE components (i.e. 531.9 and 533 eV) can be attributed to the surface oxygen bonded to carbon in the form of either carbonyl (oxygen bonded to carbon) or hydroxyl (oxygen bonded to hydrogen) groups, which were adsorbed on the sample surface as impurities during sample transfer from the fabrication chamber and/or furnace atmosphere to the XPS load lock, appear as a shoulder contribution with minor intensities.[7,37]

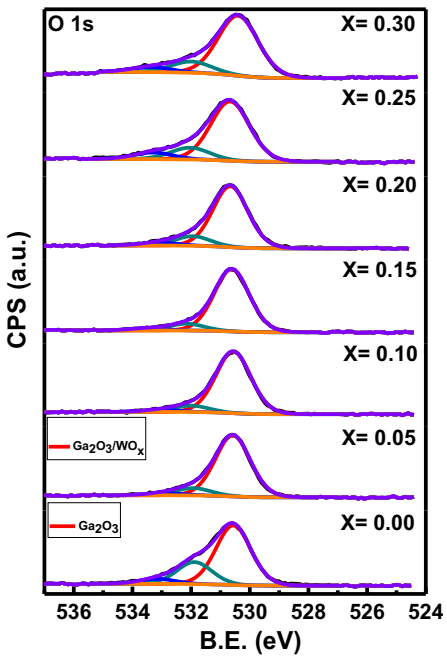

Figure 6. O 1s core-level spectra of GWO compounds.

Conclusions

$Ga_{2-2x}W_xO_3$, $0.00 \leq x \leq 0.30$, polycrystalline ceramic compounds were synthesized by the standard high-temperature solid-state chemical reaction method. The effect of W-doping is found to significant on the crystal structure and electronic structure of the resulting GWO materials. For W-content $x \leq 0.15$, single-phase GWO compounds crystallize in parent β-Ga_2O_3 while Ga_2O_3-WO_3 composite formation occurs at higher x values. The crystallite size increases from ~40 to ~50 nm with increasing W-content although most the crystallite size increase occurs in the single phase GWO compounds. Tungsten exhibits the mixed chemical valence states, W^{4+} and W^{6+}, in single-phase GWO compounds for lower x values while the fully oxidized or highest chemical valence state (W^{6+}) occurs for higher x values that correspond to the formation of Ga_2O_3-WO_3 mixed oxide. Gallium exists in their highest chemical valence state, Ga^{3+}, in all of the GWO compounds i.e., irrespective of W-doping. The fundamental understanding of the crystal structure and electronic structure modification of the GWO materials as function of W concentration could be useful while considering the W-doped Ga_2O_3 materials and/or W-Ga_2O_3 contacts for electronic and optoelectronic device applications.

Acknowledgments

The authors acknowledge, with pleasure, support from the National Science Foundation (NSF) with NSF-PREM grant #DMR-1827745. This material is also based upon work supported by the Air Force Office of Scientific Research under award number FA9550-18-1-0387. However, any opinions, finding, and conclusions or recommendations expressed in this material are those of the author(s) and do not necessarily reflect the views of the United States Air Force.

ORCID

C. V. Ramana https://orcid.org/0000-0002-5286-3065

References

1. M. Higashiwaki, K. Sasaki, A. Kuramata, T. Masui, and S. Yamakoshi, *Applied Physics Letters*, **100**(1), 013504 (2012).
2. L. Dong, R. Jia, B. Xin, B. Peng, and Y. Zhang, *Scientific Reports*, **7** 40160 (2017).
3. D. Guo, H. Liu, P. Li, Z. Wu, S. Wang, C. Cui, C. Li, and W. Tang, *ACS Applied Materials & Interfaces*, **9**(2), 1619 (2017).
4. M. A. Mastro, A. Kuramata, J. Calkins, J. Kim, F. Ren, and S. Pearton, *ECS Journal of Solid State Science and Technology*, **6**(5), P356 (2017).
5. S. Pearton, J. Yang, P. H. Cary IV, F. Ren, J. Kim, M. J. Tadjer, and M. A. Mastro, *Applied Physics Reviews*, **5**(1), 011301 (2018).
6. W. Zhou, C. Xia, Q. Sai, and H. Zhang, *Applied Physics Letters*, **111**(24), 242103 (2017).
7. R. P. Oleksak, W. F. Stickle, and G. S. Herman, *Journal of Materials Chemistry C*, **3**(13), 3114 (2015).
8. N. Suzuki, S. Ohira, M. Tanaka, T. Sugawara, K. Nakajima, and T. Shishido, *Physica Ptatus Solidi C*, **4**(7), 2310 (2007).
9. L. Fu, Y. Liu, P. a. Hu, K. Xiao, G. Yu, and D. Zhu, *Chemistry of Materials*, **15**(22), 4287 (2003).
10. S. Zhou, G. Feng, B. Wu, N. Jiang, S. Xu, and J. Qiu, *The Journal of Physical Chemistry C*, **111**(20), 7335 (2007).
11. S. Jin, X. Wang, X. Wang, M. Ju, S. Shen, W. Liang, Y. Zhao, Z. Feng, H. Y. Playford, and R. I. Walton, *The Journal of Physical Chemistry C*, **119**(32), 18221 (2015).
12. D. S. Ginley and C. Bright, *MRS Bulletin*, **25**(8), 15 (2000).
13. T. Minami, *Semiconductor Science and Technology*, **20**(4), S35 (2005).
14. M. M. Muhammed, N. Alwadai, S. Lopatin, A. Kuramata, and I. S. Roqan, *ACS Applied Materials & Interfaces*, **9**(39), 34057 (2017).
15. M. Ogita, K. Higo, Y. Nakanishi, and Y. Hatanaka, *Applied Surface Science*, **175**, 721 (2001).

16. M. Bartic, C. I. Baban, H. Suzuki, M. Ogita, and M. Isai, *Journal of the American Ceramic Society*, **90**(9), 2879 (2007).
17. Y. Li, A. Trinchi, W. Wlodarski, K. Galatsis, and K. Kalantar-zadeh, *Sensors and Actuators B: Chemical*, **93**(1-3), 431 (2003).
18. H. Peelaers and C. G. Van de Walle, *Physica Status Solidi (B)*, **252**(4), 828 (2015).
19. S. Ghose, S. Rahman, L. Hong, J. S. Rojas-Ramirez, H. Jin, K. Park, R. Klie, and R. Droopad, *Journal of Applied Physics*, **122**(9), 095302 (2017).
20. G. Yang, S. Jang, F. Ren, S. J. Pearton, and J. Kim, *ACS Applied Materials & Interfaces*, **9**(46), 40471 (2017).
21. J. Åhman, G. Svensson, and J. Albertsson, *Acta Crystallographica Section C: Crystal Structure Communications*, **52**(6), 1336 (1996).
22. T. Liu, Z. Feng, Q. Li, J. Yang, C. Li, and M. Dupuis, *Chemistry of Materials*, **30**(21), 7714 (2018).
23. E. G. Víllora, K. Shimamura, Y. Yoshikawa, T. Ujiie, and K. Aoki, *Applied Physics Letters*, **92**(20), 202120 (2008).
24. H. Peelaers and C. Van de Walle, *Physical Review B*, **94**(19), 195203 (2016).
25. A. K. Battu, S. Manandhar, and C. V. Ramana, *Materials Today Nano*, **2** 7 (2018).
26. E. J. Rubio, T. E. Mates, S. Manandhar, M. Nandasiri, V. Shutthanandan, and C. V. Ramana, *The Journal of Physical Chemistry C*, **120**(47), 26720 (2016).
27. A. Dakhel, *Journal of Materials Science*, **47**(7), 3034 (2012).
28. R. D. Shannon, *Acta Crystallographica Section A: Crystal Physics, Diffraction, Theoretical and General Crystallography*, **32**(5), 751 (1976).
29. L. Francke, E. Durand, A. Demourgues, A. Vimont, M. Daturi, and A. Tressaud, *Journal of Materials Chemistry*, **13**(9), 2330 (2003).
30. D. Chen, Y. Zhang, X. Ge, Y. Cheng, Y. Liu, H. Yuan, J. Guo, M. Chao, and E. Liang, *Physical Chemistry Chemical Physics*, **20**(30), 20160 (2018).
31. Y. Yao, R. F. Davis, and L. M. Porter, *Journal of Electronic Materials*, **46**(4), 2053 (2017).
32. Y. Yao, R. Gangireddy, J. Kim, K. K. Das, R. F. Davis, and L. M. Porter, *Journal of Vacuum Science & Technology B, Nanotechnology and Microelectronics: Materials, Processing, Measurement, and Phenomena*, **35**(3), 03D113 (2017).
33. Vishal Zade, M. Bandi, S. Sanjay, A. Bronson, and C. V. Ramana, *Inorganic Chemistry*, (2019) in press.
34. H. Kalhori, S. B. Porter, A. S. Esmaeily, M. Coey, M. Ranjbar, and H. Salamati, *Applied Surface Science*, **390** 43 (2016).
35. H. Wriedt, *Bulletin of Alloy phase diagrams*, **10**(4), 368 (1989).
36. C. Hinkle, M. Milojevic, A. Sonnet, H. Kim, J. Kim, E. M. Vogel, and R. M. Wallace, *ECS Transactions*, **19**(5), 387 (2009).
37. C. Ramana, E. Rubio, C. Barraza, A. Miranda Gallardo, S. McPeak, S. Kotru, and J. Grant, *Journal of Applied Physics*, **115**(4), 043508 (2014).
38. A. Trinchi, S. Kaciulis, L. Pandolfi, M. K. Ghantasala, Y. X. Li, W. Wlodarski, S. Viticoli, E. Comini, and G. Sberveglieri, *Sensors and Actuators B: Chemical*, **103**(1-2), 129 (2004).
39. S.-L. Ou, D.-S. Wuu, Y.-C. Fu, S.-P. Liu, R.-H. Horng, L. Liu, and Z.-C. Feng, *Materials Chemistry and Physics*, **133**(2-3), 700 (2012).